Aluminium Nitride thin Film Acoustic Wave Device for Microfluidic and Biosensing Applications

Y.Q. Fu[1], J. S. Cherng[2], J. K. Luo[3], M.P.Y. Desmulliez[1], Y. Li[4],
A. J. Walton[4] and F. Placido[5]
[1]School of Engineering and Physical Sciences, Institute of Integrated Systems,
Heriot-Watt University, Edinburgh, EH14 4AS,
[2]Department of Materials Engineering,
Mingchi University of Technology, Taishan, Taipei,
[3]Centre for Material Research and Innovation, University of Bolton,
Deane Road, Bolton, BL3 5AB,
[4] Scottish Microelectronics Centre, School of Engineering, Institute of Integrated Systems,
University of Edinburgh, Edinburgh, EH10 7AT,
[5]Thin Film Centre, University of the West of Scotland, Paisley, PA1 2BE,
[1,3,4,5]UK
[2]Taiwan

1. Introduction

When an alternating electric field is applied to an interdigitated transducer (IDT) on a piezoelectric material, an acoustic wave is generated. The wave can propagate in a direction perpendicular to the surface of the material into the bulk (bulk acoustic wave, BAW) or along the surface of the material (surface acoustic wave, SAW). This piezoelectric effect is manifested in either a Rayleigh mode (vertical and surface normal) or as a shear horizontal wave (in-plane) [Galipeau et al 1997]. The most commonly used bulk acoustic wave device is the Quartz Crystal Microbalance (QCM), which is generally made of quartz sandwiched between two electrodes. In contrast a surface acoustic wave propagating within a thin surface layer, which has a lower acoustic velocity than that of the piezoelectric substrate, is called a Love wave and such devices are typically operated in the Shear Horizontal (SH) wave mode. Waves propagating in a thin plate with a thickness much less than the acoustic wavelength are called a flexural plate or Lamb waves [Luginbuhl et al 1997]. These acoustic wave technologies and devices have been commercially exploited for more than 60 years in industrial applications [Ballantine et al 1996. Hoummady et al., 1997] and currently the telecommunications industry is one of the largest consumers, primarily in mobile phones and base stations, which account for ~3 billion acoustic wave filters annually. Other promising and growing applications include automotive applications (pressure acceleration, or shock sensors), medical applications (chemical sensors), and other industrial applications (including temperature, mass, viscosity, vapour and humidity sensors).

Most acoustic wave devices can be used as sensors because they are sensitive to mechanical, chemical, or electrical perturbations on the surface of the device [Lucklum & P. Hauptmann 2003, Grate et al 2003]. Acoustic wave sensors have the advantage that they are versatile, sensitive and reliable, being able to detect not only mass/density changes, but also viscosity, wave functions, elastic modulus, conductivity and dielectric properties. They have many applications in monitoring a large number of parameters which include pressure, moisture, temperature, force, acceleration, shock, viscosity, flow, pH, ionic contaminants, odour, radiation and electric fields [Shiokawa & Kondoh 2004, Wohltjen et al. 1997]. Recently, there has been an increasing interest in acoustic wave based biosensors to detect traces of biomolecules through specific bioreactions with biomarkers. These include DNA, proteins (enzymes, antibodies, and receptors), cells (microorganisms, animal and plant cells, cancer cells etc.), tissues, viruses, as well as the detection of chemical substances through specific chemical absorption layers [Cote et al 2003, Kuznestsova, and Coakley 2007, Teles & Fonseca 2003]. By detecting traces of associated molecules, it is possible to diagnose diseases and genetic disorders, prevent potential bioattachment, and monitor the spread of viruses and pandemics [Vellekoop 1998, Shiokawa & Kondoh 2004, Gizeli 1997]. Compared with other common bio-sensing technologies, such as surface plasmon resonance (SPR), optical fibres, and sensors based on field effect transistors or cantilever-based detectors, acoustic wave based technologies have the combined advantages of simple operation, high sensitivity, small size and low cost, with no need for bulky optical detection systems [Lange et al 2008].

By far the most commonly reported acoustic wave based biosensor is QCM [Markx, 2003], which can be operated in a liquid environment using a thickness shear-mode. The advantages of QCM include: (1) simplicity in design and (2) a high Q factor. However, less attractive features of QCM biosensors are a low detection resolution due to the low operating frequency in the range of 5~20 MHz and a large base mass; a thick substrate (0.5~1 mm) and large surface area (>1 cm^2) which cannot easily be scaled down. In contract SAW based biosensors have their acoustic energy confined within a region about one wave length from the surface, and so the basemass of the active layer is roughly one order of magnitude smaller than that of the QCM. Therefore, the sensitivity of the SAW devices is dramatically larger than that of the QCM. The longitudinal or Rayleigh mode SAW device has a substantial surface-normal displacement that rapidly dissipates the acoustic wave energy into the liquid, leading to excessive damping, and hence poor sensitivity and noise. However, waves in a SH-SAW device propagate in a shear horizontal mode, and therefore do not easily radiate acoustic energy into the liquid [Barie & Rapp 2001, Kovacs & Venema 1992] and hence the device maintains a high sensitivity in liquids. Consequently SH-SAW devices are particularly well suitable for bio-detection, especially for "real-time" monitoring. In most cases, Love wave devices operate in the SH wave mode with the acoustic energy trapped within a thin waveguide layer (typically sub-micron). This enhances the detection sensitivity by more than two orders of magnitude compared with a conventional SAW device owing to their much reduced base mass [Josse et al 2001, Mchale 2003]. They are therefore frequently employed to perform biosensing in liquid conditions [Lindner 2008, Kovacs et al 1992, Jacoby & Vellekoop 1997].

Acoustic wave technologies are also particularly well suited to mixing and pumping and as a result are an attractive option for microfluidics applications [Luo et al 2009]. Taking the SAW device as one example, Rayleigh-based SAW waves have a longitudinal component that can be coupled with a medium in contact with the surface of the device. When liquid

(either in bulk or droplet form) exists on the surface of a SAW device, the energy and momentum of the acoustic wave are coupled into the fluid with a Rayleigh angle, following Snell's law of refraction (see Fig. 1) [Wixforth 2004, Shiokawa et al 1989]. The Rayleigh angle, θ, is defined by

$$\theta = \sin^{-1}\left(\frac{v_l}{v_S}\right)$$ (2)

where v_l and v_s are the velocities of the longitudinal wave in solid and liquid. The generated acoustic pressure can create significant acoustic streaming in a liquid which can be used to enable liquid mixing, pumping, ejection and atomization [Newton et al 1999]. This pressure facilitates rapid liquid movement and also internal agitation, which can be used to speed up biochemical reactions, minimize non-specific bio-binding, and accelerate hybridization reactions in protein and DNA analysis which are routinely used in proteomics and genomics [Toegl et al 2003, Wixforth et al 2004]. Surface acoustic wave based liquid pumps and mixers [Tseng et al 2006, Sritharan et al 2006], droplet positioning and manipulation [Sano et al 1998], droplet ejection and atomization systems [Chono et al 2004, Murochi et al 2007], and fluidic dispenser arrays [Strobl et al 2004] have been proposed and developed. They have distinct advantages, such as a simple device structure, no moving-parts, electronic control, high speed, programmability, manufacturability, remote control, compactness and high frequency response [Renaudin et al 2006, Togle et al 2004, Franke & Wixforth 2008].
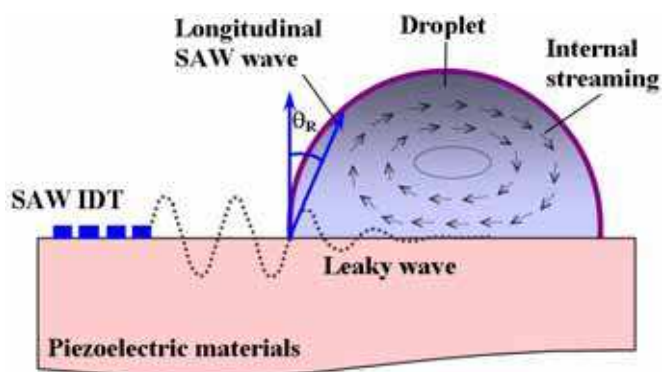

Fig. 1. Principle of surface acoustic wave streaming effect: interaction between propagating surface acoustic wave and a liquid droplet causing acoustic streaming inside droplet

Acoustic wave devices can be used for both biosensing and microfluidics applications, which are two of the major components for lab-on-a-chip systems. Therefore, it is attractive to develop lab-on-chip bio-detection platforms using acoustic wave devices as this integrates the functions of microdroplet transportation, mixing and bio-detection. To date, most of the acoustic devices have been made from bulk piezoelectric materials, such as quartz (SiO_2), lithium tantalate ($LiTaO_3$), lithium niobate ($LiNbO_3$) and sapphire (Al_2O_3). These bulk materials are expensive, and are less easily integrated with electronics for control and signal processing. Piezoelectric thin films such as PZT, ZnO and AlN have good

piezoelectric properties, high electro-mechanical coupling coefficient, high sensitivity and reliability [Pearton et al 2005]. They can be grown in thin film form on a variety of substrates, which include silicon, making these materials promising for integration with electronic circuitry, particularly for devices aimed for one-time use, low-price and mass production [Muralt 2008] (see Table 1). Amongst these, PZT has the highest piezoelectric constant and electromechanical coupling coefficient. However, for biosensing applications, PZT films have disadvantages such as higher acoustic wave attenuation, lower sound wave velocities, poor biocompatibility and worst of all, the requirement for extremely high temperature sintering and high electric field polarization, which make them largely unsuitable for integration with electronics (see Table 1). ZnO shows a high piezoelectric coupling, and it is easy to control the film stoichiometry, texture and other properties compared with that for AlN film [Jagadish & Pearton 2006]. Zinc oxide is considered

Materials	ZnO	AlN	PZT	Quartz	128° cut LiNbO$_3$	36° cut LiTaO$_3$	PVDF
Density (g/cm^3)	5.61	3.3	7.8	2.64	4.64	7.45	1.79
Moulus (GPa)	110-140	300-350	61	71.7		225	0.16
Hardness	4-5 GPa	15 GPa	7-18 GPa	Moh's 7	Moh's 5 Knoop 800-1000	70-110 Knoop 700-1200	Shore D75-85
refractive index	1.9 to 2.0	1.96	2.40	1.46	2.29	2.18	1.42
Piezo-constant d33 (pC/N)	12	4.5, 6.4	289-380, 117	2.3(d11)	19-27	-21	-35
Coupling coefficient, k	0.15-0.33	0.17-0.5	0.49	0.0014	0.23	0.2	0.12-0.2
Effective coupling coefficient, k^2 (%)	1.5-1.7	3.1-8	20-35	8.8-16	2-11.3	0.66-0.77	2.9
Acoustic velocity by transverse (m/s)	6336 (2650)	11050 (6090)	4500 (2200)	5960 (3310)	3970	3230-3295	2600
Dielectric constant	8.66	8.5-10	380	4.3	85 (29)	54 (43)	6-8
Coefficient of thermal expansion (CTE, x10^{-6})	4	5.2	1.75	5.5	15	-16.5	42-75

Table 1. Comparison of common piezoelectric materials [Fu et al 2010]

biosafe and therefore suitable for biomedical applications that immobilize and modify biomolecules [Kumar & Shen 2008]. A summary of the recent development on ZnO film based microfluidics and sensing have been reported by Fu et al 2010. Currently, there is some concern that ZnO film is reactive, and unstable even in air or moisture and the stability and reliability is potentially a major problem.

AlN has a very large volume resistivity and is a hard material with a bulk hardness similar to quartz, and is also chemically stable to attack by atmospheric gases at temperatures less than 700°C. Compared with ZnO, AlN also shows a slightly lower piezoelectric coupling. However, the Rayleigh wave phase velocity in AlN is much higher than that in ZnO, which suggests that AlN is better for high frequency and high sensitivity applications [Lee et al 2004]. The combination of its physical and chemical properties is consequently promising for practical applications of AlN both in bulk and thin-film forms. Using AlN potentially enables the development of acoustic devices operating at higher frequencies, with improved sensitivity and performance (insertion loss and resistance) in harsh environments [Wingqvist et al 2007a]. AlN thin films have other attractive properties such as high thermal conductivity, good electrical isolation and a wide band gap (6.2 eV). Therefore, AlN thin films have been used, not only for the surface passivation of semiconductors and insulators, but also for both optical devices in the ultraviolet spectral region and acousto-optic devices.

This chapter will focus on reviewing recent progress covering the issues related to AlN film preparation, its microstructure, piezoelectric properties and device fabrication as well as applications related to microfluidcis and biosensing.

2. AlN film processing and characterization

The AlN crystal belongs to a hexagonal class or a distorted tetrahedron (see Fig. 2), with each Al atom surrounded by four N atoms [Chiu et al 2007]. The four Al–N bonds can be categorized into two types: three are equivalent Al–N$_{(x)}$ (x = 1, 2, 3) bonds, B$_1$, and one is a unique Al–N bond, B$_2$, in the *c*-axis direction or the (002) orientation. Since the B$_2$ is more ionic, it has a lower bonding energy than the other bonds [Chiu et al 2007]. The highest value of K_t^2 and the piezoelectric constant are in the *c*-axis direction, thus the AlN film growing with *c*-axis orientation has much better piezoelectricity when an acoustic wave device is excited in the film thickness direction.

2.1 AlN deposition methods

Many different methods have been used to prepare AlN films. These include chemical vapour deposition (CVD) or plasma enhanced CVD (PECVD) [Sanchez et al 2008, Tanosch et al 2006, Ishihara et al 2000, Liu et al 2003], filtered arc vacuum arc (FAVC) [Ji et al 2004], molecular beam deposition (MBE) [Kern et al 1998], hydride vapour phase epitaxy (HVPE) [Kumagai et al 2005], pulsed laser deposition (PLD) [Lu et al, 2000, Liu et al 2003, Baek et al 2007], and sputtering [Mortet et al 2003 and 2004, Auger et al 2005, Clement et al 2003]. Of these technologies, MBE can grow a single-crystal epitaxial AlN film with other advantages which include precise control over the deposition parameters, atomic scale control of film thickness and *in situ* diagnostic capabilities. However, it has limitations of low growth rate, expensive instrument setup and a high process temperature from 800 to 1000°C. Unfortunately this results in thermal damage of the AlN layers during deposition, as well as the substrate depending on the material. CVD technology including metal organic CVD

(MOCVD) and PECVD is also of great interest for AlN film growth because it not only gives rise to high-quality films but also is applicable to large-scale production. However, its high process temperature (about 500 to 1000 °C) may be inappropriate for CMOS-compatible processes and this causes large thermal stresses in the films, which potentially restricts the choice of substrate. The main advantages of PLD are its ability to create high-energy source particles, permitting high-quality film growth at potentially low substrate temperatures (typically ranging from 200 to 800 °C) in high ambient gas pressures in the 10^{-5}–10^{-1} Torr range. One disadvantages of PLD is its limited deposition size and uniformity.
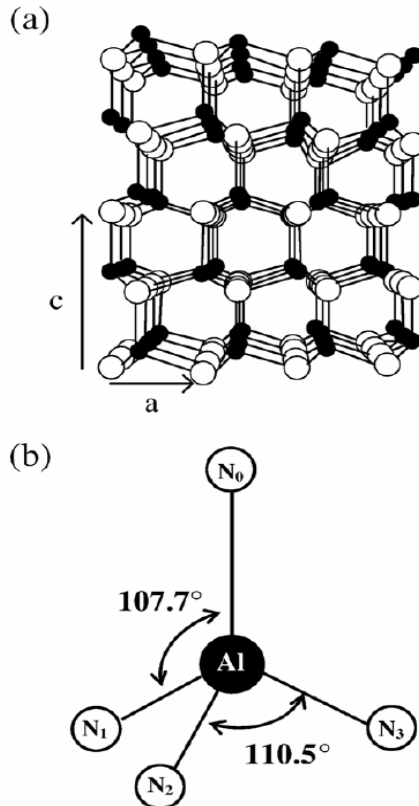
Fig. 2. (a) Hexagonal structure of AlN and (b) tetrahedral structure, with one Al atom surrounded by four N atoms [Chiu et al 2007].

One of the most popular thin film deposition techniques for AlN films is sputtering (DC, radio-frequency magnetron and reactive sputtering). They can be deposited in an N_2/Ar reactive atmosphere by DC reactive sputtering pure Al, or by RF sputtering using an AlN target. Sputtering methods can deposit a good crystalline AlN thin film at a relatively low temperature (between 25 °C and 500 °C) and the sputtered films normally exhibit good epitaxial film structure [Engelmark et al 2000]. DC Sputtering using an Al target can result in "target poisoning" caused by the accumulation of charging on the target, which causes arcing or a decrease in the sputtering rate. Switching the choice of power supply from DC to

RF addresses this problem, but at the cost of lower deposition rate and more expensive and complex equipment. Pulsed-DC reactive sputtering provides a solution to this limitation and also brings other advantages, which include higher film uniformity and higher plasma activity [Cherng et al. 2007, 2008].

From a MEMS fabrication point of view, reactive sputtering is one of the best methods, with good reproducibility and compatibility with planar device fabrication technology. In this section, we will focus on the processing, texture and acoustic wave properties of the sputtered AlN films.

2.2 Influence of process parameters

The quality of the sputtered AlN thin films depends on plasma power, working pressure, substrate temperature, RF power and substrate materials. Increasing the RF power causes higher kinetic energy of adatoms when they arrive on the substrate, which provides enough energy for the formation of the (0 0 0 2) preferred orientation of AlN layers. On the other hand, increased RF power also raises the number of ejected species from the target, which results in an increased growth rate as a function of RF power.

Gas pressure potentially also has a significant influence on AlN film deposition with increasing the sputtering pressure up to 1.33 Pa being reported to improve the crystalline quality of the (0 0 0 2)-oriented AlN layers. However, it was also noted that further increases in the sputtering pressure degraded the crystalline quality [Gao et al 2007]. Increasing in the sputtering pressure will raise the probability of collisions between sputtered particles and nitrogen atoms simply because of more gas atoms are available for ionization. Therefore, the average energy of the sputtered particles is increased which improves the crystalline quality. However, further increase in sputtering pressure results in the reduction of mean free path of N or Ar ions, which leads to a reduction of the energy of sputtered and deposited atoms, thus degrading the crystalline quality [Gao et al 2007].

Okamoto et al 2000 observed a change of the preferred crystallographic orientation by increasing the N_2 partial pressure, and Baek et al. 2007 detected the same effect when the substrate temperature and N_2 gas fluence were changed. Sudhir et al. 1998 demonstrated that the surface morphology and structure of the AlN films can be actively controlled by adjusting the nitrogen partial pressure during the film deposition. They attributed the observed dependence of the structural quality to the change in the surface diffusion of adatoms, given by $L \sim (D\tau)^{1/2}$, where D is the diffusion coefficient and τ is the residence time of adatoms. Larger values of diffusion length imply more time for the adatoms to find energetically favourable lattice positions, thus reducing the density of surface defects and improving the crystal quality [Sudhir et al 1998].

Leong and Ong 2004 prepared reactive magnetron sputtered AlN films by varying parameters such as substrate temperature Ts, radio frequency power Pw, and substrate materials (including silicon, platinum coated silicon and sapphire). The effects of these parameters on film microstructure as a function of deposition temperature are shown in Fig. 3. This identifies the regions of nearly amorphous (na-) AlN, polycrystalline (p-) AlN, texture (t-) AlN and epitaxial (e-) AlN on three substrate materials, i.e. Si(100), Pt(111)/Si(100) and Al_2O_3(001), respectively. The 'na-AlN" means that the microstructure of AlN has a highly disordered matrix containing small randomly orientated crystals, which normally forms at a lower rf power, and low temperature [Leong & Ong 2004]. At higher temperature and power, the thermal energy gained by the depositing species is larger, and the atoms are more mobile. Hence, the species more readily aggregate and crystallize,

resulting in the formation of larger grains compared with those present in the na-AlN structure. Increases in *Ts* and *Pw* have the effects of increasing the thermal energy of the species on the substrate surface, and enhancing the crystallization of the deposits and preferential orientation of grains. It should be noted that sapphire substrate have better lattice matching with the AlN, which facilitates the epitaxial growth of the AlN structure [Leong & Ong 2004].
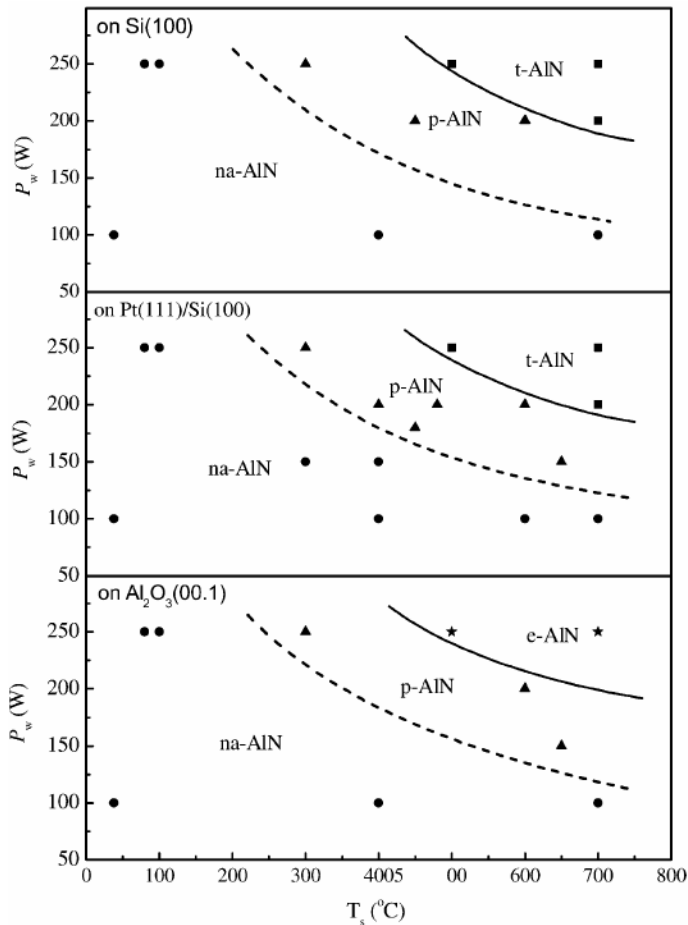

Fig. 3. Effects of the process parameters on film microstructure on three substrate materials, i.e. Si(100), Pt(111)/Si(100) and Al$_2$O$_3$(001) [Leung & Ong 2004]

Because of the reactivity of Al, a high-purity source Al material and an oxygen-free environment are required to grow high-quality AlN film [Vashaei et al 2009]. Hence, oxygen has a significant influence on AlN film growth during sputtering, and contamination due to residual oxygen or water can seriously interfere with the formation of the AlN film structure. Growth rate of the AlN film decrease with increased oxygen in the sputtering gas and their predominant polarity also changes from Al polarity to N polarity with increase in

the oxygen concentration [Vergara et al 2004, Cherng et al 2008 a and b]. Increased oxygen concentration in sputtering gas increases Al-O bonding, as the bonding energy of Al-O (511 kJ/mol) is higher than that of Al-N (230 kCal/mol) [Akiyama et al 2008], and formation of Al-O bond significantly deteriorates the piezoelectric response of the AlN films.

The quality of AlN films is affected by any contamination during sputtering [Cheung & Ong 2004], resulting from target impurity, gas impurity, and residual oxygen/moisture from both inside (adsorption) and outside (leakage) the working chamber. Out-gassing is a critical parameter that must be controlled for quality of AlN crystals, and effect of the out-gassing rate has been evaluated by observing the pressure increase with time after the designated base pressure has been reached and the pump was shut down (as shown in Fig. 4). The FWHM (full width of half maximum) from an X-ray diffraction rocking curve and the residual stress of the films has been obtained in order to compare the film quality [Cherng 2008 and 2009].
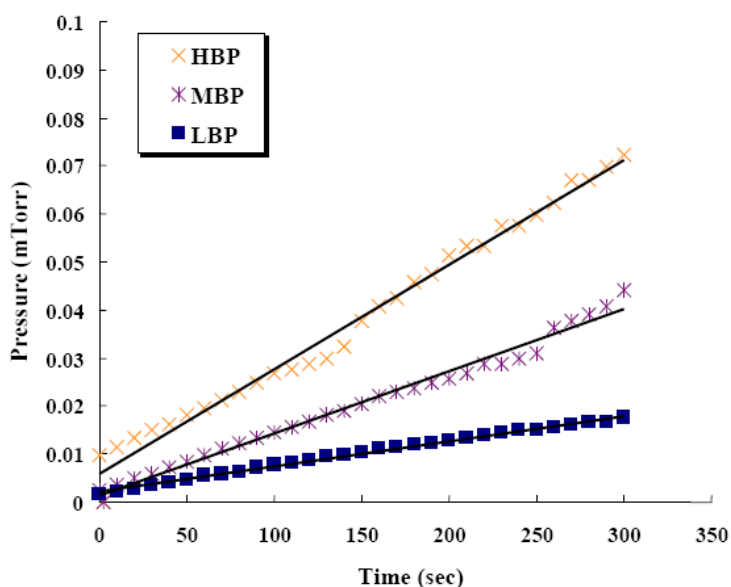

Fig. 4. Outgassing rate evaluated by observing the pressure increase with time after the designated base pressure was reached and the pump was shut down where the slope of each curve indicates its outgassing rate respectively. The sputtering system was either pumped down to a base pressure of 3×10^{-6} Torr (thus termed HBP, high base pressure) or 1×10^{-6} Torr (thus termed MBP, medium base pressure) or 4×10^{-7} Torr (thus termed LBP, low base pressure) before admitting the gas mixture in, in order to examine the effects of outgassing [Cherng & Chang, 2008]

Figures 5(a) and (b) show the effect of working pressure on FWMH and film stress at different outgasing levels. The FWHM decreases and residual stress becomes more compressive with decreasing working pressure. As the pressure is decreased, the mean free path of the sputtered atoms becomes comparable with the target-to-substrate distance ($\lambda_{mfp}=5 / P$, where λ_{mfp} is in cm and P in mTorr) [O'Hanlon 1989], and hence less gas phase scattering is observed. The result is that sputtered Al atoms arrive on the surface of the

growing film with most of their energy retained. They transfer a substantial amount of energy to the growing film, and thus increase the mobility of the adatoms and can then move to the lattice sites which form a closest-packed (0002) plane with the lowest surface energy. In fact, the energy delivered to the growing film is sufficiently high so that fully (0002)-textured (texture coefficient=1) AlN films with FWHM of the rocking curve lower than 2° are readily obtainable without substrate heating. In addition to the aforementioned "atom-assisted deposition" [Iriarte et al 2002], a second mechanism, namely, "atomic peening" [Windischmann 1992] is also at work. Since N atoms are lighter than Al, the reflection coefficient of N ions is high sufficient for a large fraction of them bombarding the Al target to be neutralized and reflected off the target surface upon impact. This results in additional bombardment of the growing film by energetic N neutrals. On the other hand, Ar ions are effectively not reflected since they are heavier than Al. Both the atom assisted deposition and atomic peening mechanisms require a sufficiently low working pressure so the energetic particles do not lose much of their energy while travelling through the gas phase. This explains why as the working pressure decreases, the FWHM of the rocking curve decreases and the residual stress becomes more compressive [Cherng & Chang, 2008]. Lower outgassing levels show a better figure-of-merit that not only the FWHM of the rocking curve is lower, but also the change of residual stress with pressure occurs in a much smoother manner and with much smaller magnitude. X-ray Photoelectron Spectroscopy (XPS) analyses for four selected samples circled in Fig. 5(a), reveal higher oxygen contents for samples with higher outgassing. SEM observations show thinner and slanter columnar structure in the AlN film when outgassing is higher upon sputtering. Both of the lower residual stress levels and the lower FWHM values at lower outgassing can be attributed to oxygen-related extended defects [Cherng & Chang, 2008].

Figure 5 © shows the relationship between FWHM and pressure at different target-to-substrate distances. At a longer target-to-substrate distance, the insensitive region shrinks and the threshold value shifts to a lower pressure [Cherng & Chang, 2008]. This is due to the decreasing ratio of mean free path to target-to-substrate distance, indicating more gas phase scattering and thus worse film quality.

With increasing nitrogen concentration, atomic peening is favoured while atom-assisted deposition basically remains unaffected. The former explains the decreasing FWHM values and more compressive stress with increasing N_2 %, as shown in Figs. 6(a) and (b). At a lower base pressure, the influence of atmospheric composition diminishes to such an extent that the FWHM of the rocking curve practically stays the same between 20 and 90 % N_2. This finding, together with the insensitive FWHM vs. pressure regions (see Fig. 6) reveal that oxygen contamination is the most dominant factor for the film properties. In the other hand the residual stress at lower outgassing rates varies little with nitrogen content. The oxygen related extended defects are deductive to compressive stress, instead of tensile stress, which is normally caused by re-sputtering type of defects. As seen in Fig. 6(c), the FWHM of the rocking curve decreases with increasing substrate temperature. This is consistent with the higher mobility of adatoms at higher substrate temperatures. Once again, the behaviour at lower outgassing becomes insensitive with substrate temperature. At this point, it is worth noting that at low outgassing, a somewhat "insensitive" region and/or a so-called "threshold" behaviour exists with all process-related parameters, e.g., working pressure, atmosphere composition, and substrate temperature. This emphasizes the crucial role oxygen contamination plays in pulsed-DC reactive sputtering of AlN thin films.
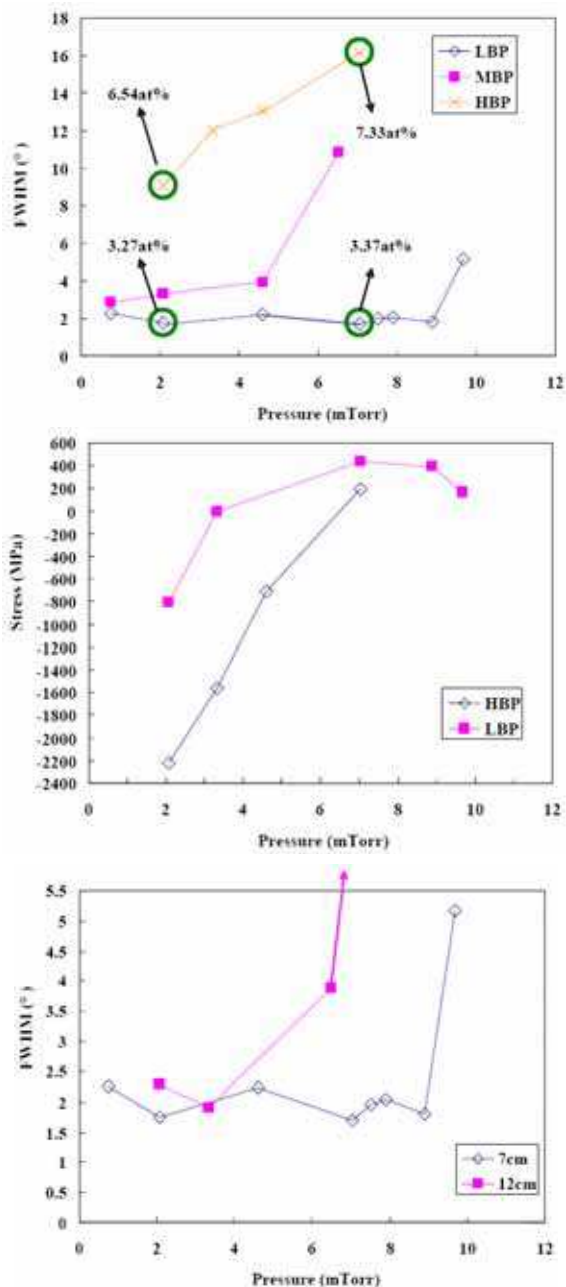
Fig. 5. Effect of working pressure on (a) XRD FWHM; and (b) film stress at various outgassing levels; and (c) on XRD FWHM at various target-to-substrate distances [Cherng et al 2008].
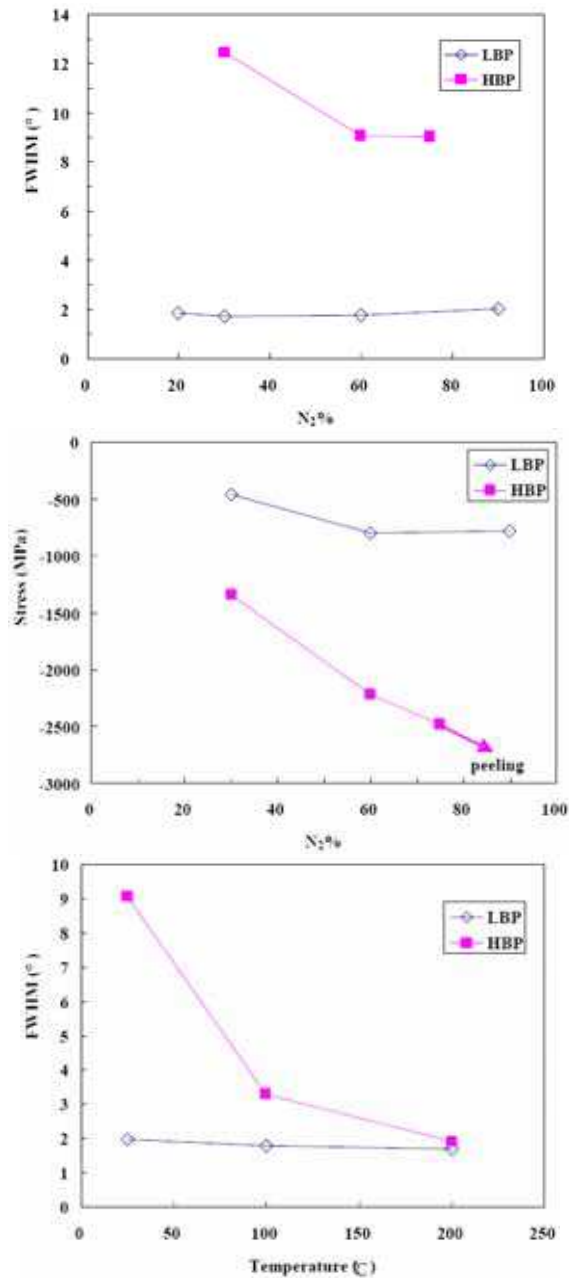
Fig. 6. Effect of atmospheric composition on (a) XRD FWHM (b) residual stress at various outgassing levels; (c) effect of substrate temperature on XRD FWHM at various outgassing levels [Cherng et al 2008].

2.3 Two-step deposition

The growth dynamic or surface kinetic roughening of the sputtered AlN films grown on Si (100) substrates has been thoroughly studied, and a two-stage growth regime identified [Auger et al 2005]. In the first step, the growth dynamic is unstable with significant sticking probabilities of the impinging particles. The films have a mixture of well textured and randomly oriented crystals. In the second regime, the films are homogeneous and well textured, and the growth is dominated by the shadowing effect induced by the bombardment of impinging particles [Auger et al 2005]. Based on this effect, a two-step pulsed-DC reactive sputtering model has been proposed with various process parameters including working pressure, discharge power, and reactive atmosphere during two stage sputtering [Cherng et al 2008, 2009]. Two-step sputtering for an AlN piezoelectric layer generally consists of a 10-min deposition for the base layer and a subsequent 50-min sputter for the top layer. As a comparison, one-step sputtering (60 min) has also been conducted with the same sputter parameters as those used for the base layer in two-step sputtering.

2.3.1 Two-step working pressure method

Figure 7 shows the effects of working pressure on (a) XRD FWHM, and (b) residual stress of AlN piezoelectric layer for both one-step and two-step sputtering, respectively. The data for two-step sputtering, when compared to their one-step counterparts, show a better figure-of-merit in that not only the FWHM of the rocking curve is smaller, but also the magnitude of the residual stress is smaller and its variation with pressure is smoother [Cherng et al 2008]. If we attribute the first step sputtering to initial nucleation and the second step to the subsequent growth of the AlN film, then the better film quality for two-step sputtering (when compared to its one-step counterpart with the same process parameters used for the base layer) has to be due to the sputtering conditions for the growth of the top layer [Cherng et al 2008]. Therefore, as far as the rocking curve width and residual stress are concerned, it is fair to say that growth, instead of nucleation, dominates the performance of two-step working pressure method.

For the AlN film deposited on Mo substrates, the FWHM values for both the 1-step and 2-step methods do not vary with working pressure and remain at the same low value of about 1.3° as shown in Fig. 7 (a) [Cherng et al 2008]. This is further confirmed by Fig. 7(b), where both the 1-step and 2-step methods using Mo substrates show low residual stress, regardless of the working pressure.

2.3.2 Two-step power method

For one-step sputtering on Si, the FWHM of the rocking curve decreases with increasing discharge power as shown in Fig. 8. This is due to the enhanced atom-assisted deposition and atomic peening mechanisms at a higher power. The sputter yield (at higher discharge voltage) and plasma concentration (more ionized species at higher discharge current) have been increased. Growth, instead of nucleation, dominates the performance of two-step power method on Si, because the data of two-step sputtering are much better than that of its one-step counterpart as also shown in Fig. 8 [Cherng et al 2009].

2.3.3 Two-step nitrogen concentration method

With increasing nitrogen concentration, atomic peening is favoured while atom-assisted deposition remains unaffected. For one-step sputtering on Si, this enhanced atomic peening
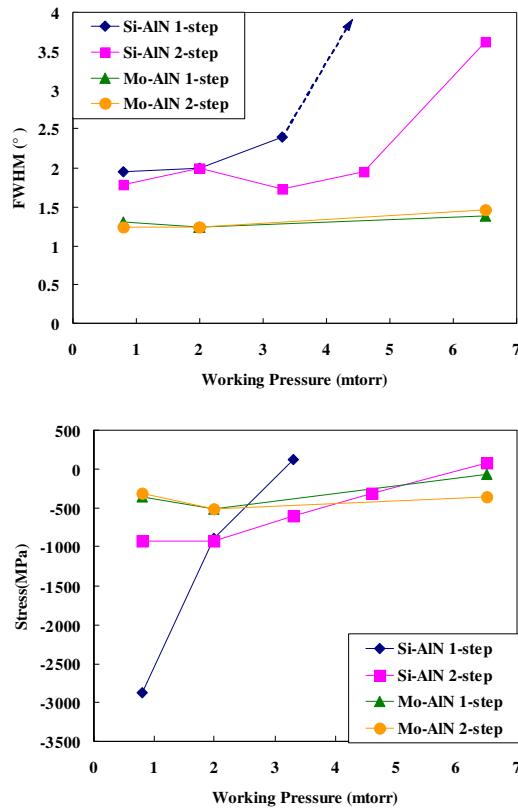
Fig. 7. Effects of working pressure on (a) XRD FWHM, and (b) residual stress of AlN
piezoelectric layer for both one-step and two-step sputtering, respectively [Cherng et al 2008]
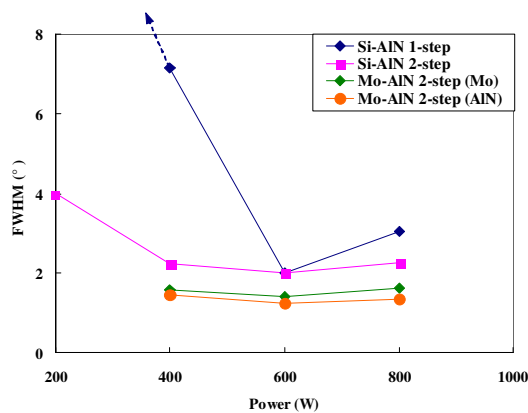

Fig. 8. Effects of discharge power on XRD FWHM for both one-step and two-step sputtering
[Cherng et al 2009].

is thought to be responsible for the decreasing FWHM of the rocking curve from 40 to 60 % of N_2, as shown in Fig. 9. The higher FWHM value at 100 % N_2 is probably due both to the excess atomic peening (causing re-sputtering) and to the worsened sputter yield (since N has a lower sputter yield than Ar). It is worth noting that the target does not exhibit any hysteresis-related phenomenon even under pure nitrogen. The employment of pulsed power is believed to be able to clean up the surface of the Al target effectively [Cherng et al 2009]. On the other hand, the FWHM behaviour for the two-step atmosphere method on Si seems to be mostly determined by initial nucleation rather than subsequent growth. The data for this is much closer to those of the one-step counterparts which employ the same sputtering conditions for the base layer. This phenomenon is just the opposite to the one observed for the other two-step methods described above, and has to be closely related to the atomic peening mechanism. It is thought that in the case of lighter bombarding particles (N atoms for atomic peening vs. Al atoms for atom assisted growth), the sputtering conditions for subsequent growth are not appropriate to alter the effects of the initial nucleation [Cherng et al 2009]. For deposition on Mo, once again, the quality of the AlN piezoelectric film is dominated by the underlying Mo film, regardless of the reactive atmosphere, as evidenced by the two-step sputtering data of the AlN and Mo films.

In conclusion, a methodology of two-step pulsed-DC reactive sputtering has been systematically evaluated for making (0002)-textured AlN thin films with independent control of rocking curve width and residual stress. This methodology was best demonstrated by the two-step working pressure method on Si, which was capable of reactively sputtering AlN thin films with almost constant rocking curve widths of about 2°, with a constant deposition rate of about 36 nm/min, and a continuously adjustable residual stress between −926 and −317 MPa [Cherng et al 2008 and 2009]. In addition, it was noted that growth dominated the performances of both the two step working pressure method and the two-step power method, while nucleation dominated the two-step atmosphere method.
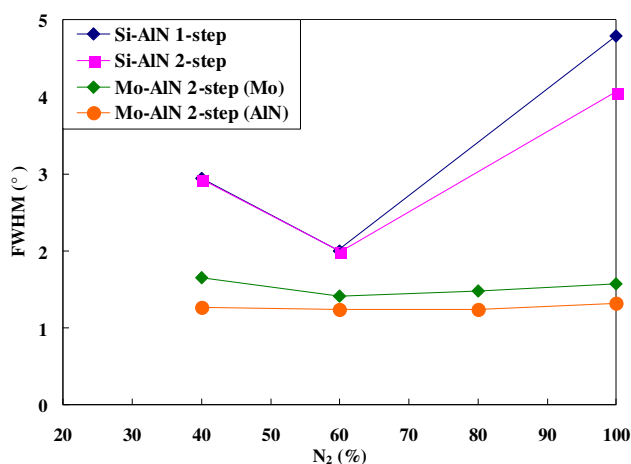

Fig. 9. Effects of reactive atmosphere on XRD FWHM for both one-step and two-step sputtering [Cherng et al 2009].

3. Piezoelectric properties of sputtered AlN films

3.1 Film thickness effect

For a SAW device made on a very thin AlN film (less than a few hundreds of nanometers), the acoustic wave can penetrate much deeper into the substrate as the film thickness is normally much less than one wavelength. In this case, the energy of a SAW device is largely dissipated in the substrate where the wave predominantly propagates. Therefore, the wave velocity of the SAW approaches the Rayleigh velocity of the substrate material as shown in Fig. 10(a) [Clement et al 2003, 2004]. When the AlN film thickness is increased, the acoustic velocity gradually changes to that of AlN film. However, there is normally a cut-off thickness, below which no wave mode can be detected, due to the low electromechanical coupling coefficient for a very thin AlN film. A Rayleigh-type wave (called the fundamental mode or mode 0) can be generated when the film is thin. With increasing film thickness, a higher order acoustic wave mode known as the Sezawa wave (mode 1) can be obtained. A Sezawa mode is realized from a layered structure in which the substrate has a higher acoustic velocity than the overlying film. This wave exhibits a larger phase velocity (higher resonant frequency) than the Rayleigh wave for a fixed thickness, and is thus desirable for high frequency applications. In a similar manner to that of Rayleigh wave, the resonant frequency and the phase velocity of the Sezawa wave decreases with film thickness. There are other higher order acoustic wave modes (modes 2 and 3, etc.) as shown in Fig. 10(a) [Clement et al 2003].

There are two key issues for the piezoelectric properties of the AlN acoustic wave device: the electro-mechanical coupling coefficient k_{eff}^2 and the quality factor Q. The effective coupling coefficient (k_{eff}^2) is related to the relative spacing between the resonant frequency and the parallel resonant frequency, and it determines the bandwidth for a band-pass filters. Fig 10 (b) shows the effective coupling coefficients of different wave modes as a function of the thickness ratio of the electrode-to-piezoelectric layers for AlN thin-film resonators [Clement et al 2003]. The quality factor Q is determined by the energy conversion efficiency from electrical into mechanical energy. However, improving one of those two parameters can cause a decrease of the other one, therefore, it would be necessary to optimize both parameters using one figure of merit (FOM), defined by the product of $k_{eff}^2 \times Q_D$ [Grate 2000].

3.2 Effects of electrodes

For an AlN based acoustic wave device, parameters such as the Q factor, resonant frequency and effective coupling constant are determined by the film and electrode material quality, as well as the electrode thickness and film roughness [Lee et al 2002]. Common used electrode materials include (111) oriented face centered cubic (fcc) metals such as Al, Pt and Ni, (110) oriented body centered (bcc) materials like Mo and W, and hexagonal metals with a (002) orientation including Ti and Ru [Lee et al 2004]. Some commonly used electrode materials for AlN SAW devices include Mo, W, Ti, Al, Au, Pt, Ni and TiN, and Ag, Co, Cr, Cu Fe, Nb, Ni, Zn, Zr have also been reported as electrodes for these acoustic wave devices [Lee et al 2004, Akiyama et al 2004]. Metallic electrodes can help promote the growth of highly *c*-axis oriented AlN films., and they can also contribute to the confinement of the mechanical energy in the piezoelectric layer at the resonant frequency. A high acoustic impedance mismatch between the piezoelectric layer and the electrodes is normally preferred, thus for this purpose, the heavy and stiff metals are the candidates of choice.
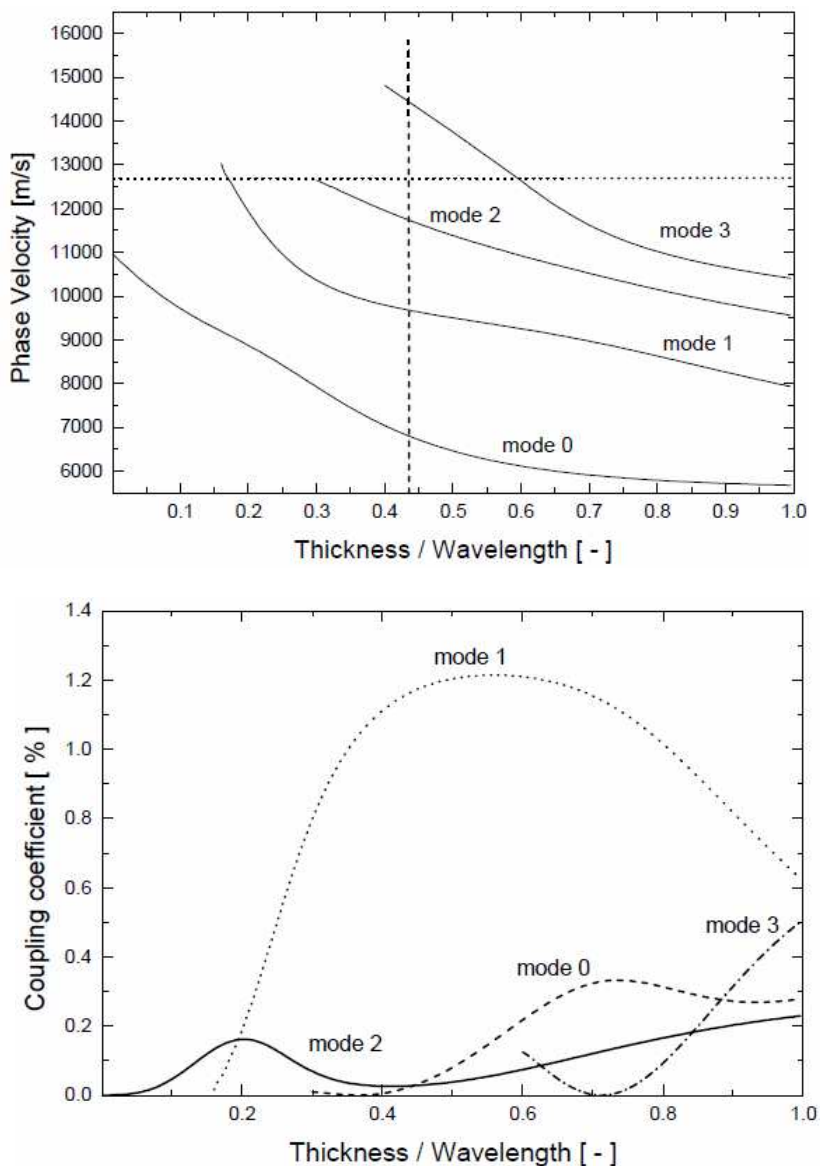
Fig. 10(a). Phase velocity for AlN film as a function of thickness/wavelength ratio for different acoustic wave modes (b). Effective coupling coefficient as a function of thickness ratio of electrode-to-piezoelectric layers for AlN thin-film resonators [Clement et al 2003].

Gold electrodes show the best resonant characteristics. The characteristics of Ag and Cu electrodes are very close to those obtained for gold, but much cheaper. Al and Mo have low resistivity and high Q factors with Mo being one of the most reported electrodes in the AlN film based acoustic devices, because it promotes the growth of highly textured AlN films

Thank You for previewing this eBook

You can read the full version of this eBook in different formats:

- ➢ HTML (Free /Available to everyone)

- ➢ PDF / TXT (Available to V.I.P. members. Free Standard members can access up to 5 PDF/TXT eBooks per month each month)

- ➢ Epub & Mobipocket (Exclusive to V.I.P. members)

To download this full book, simply select the format you desire below